

Structure-Optimized Interpolymer Polyphosphazene Complexes for Effective Gene Delivery against Glioblastoma

Wei-Hsin Hsu, Pilar Sánchez-Gómez, Esther Gomez-Ibarlucea, Delyan P. Ivanov, Ruman Rahman, Anna M. Grabowska, Noemi Csaba, Cameron Alexander,* and Marcos Garcia-Fuentes*

Safe and efficient gene delivery vectors will enhance the prospects for polynucleotide-based therapies. Herein a new approach toward structurally optimized gene vector design based on the preparation of clickable poly(allylamino-phosphazene)s that can be converted to several cationic and anionic derivatives via thiol–ene addition is described. Simultaneous co-incubation of alkylamine- and alkylcarboxylate-poly(phosphazenes) with polynucleotide generates binary polyelectrolyte nanoparticles. Screening of a series of these complexes for transfection in glioblastoma cells shows that the inclusion of 6-mercaptohexanoic acid substituted poly(phosphazene)s in the complexes results in six-fold and 19-fold higher luciferase expression in U87MG cells and GBM1 primary cells, respectively. This effect is attributed to the specific ionization properties of these materials that improved polyplex intracellular trafficking. Transfection in 3D-spheroid models and subcutaneous xenograft U87MG tumors confirms higher transgene expression for the binary cationic/anionic poly(phosphazene) complexes compared to the related polycation-pDNA complexes and to PEI-pDNA complexes. The data also indicate a notable capacity of the mixed complexes to deliver genes to the inner cores of tumor spheroids. Extension of this approach to siRNA delivery shows that the mixed poly(phosphazene) complexes can silence DYRK1A, a gene implicated in glioblastoma initiation and progression, reducing U87MG cell renewal in vitro and delaying tumor growth in vivo.

1. Introduction

Therapies based on polynucleotides offer much promise but require more efficient and safer gene carriers.^[1] While viral-based gene delivery is the most advanced in terms of the number of clinical trials,^[2] there are still concerns over the long-term safety of viral vectors, and many of the new RNA-based drugs are not easy to integrate in virus-based delivery constructs. Non-viral systems such as polymer-based gene vehicles have provided a number of promising results, but there remain several limitations for their generalized application.^[3] Design criteria that remain unfulfilled by most synthetic polymer gene carriers include a) biocompatibility and tunable biodegradability, b) selective biodistribution and adequate pharmacokinetics, c) ability to surmount tissue and extracellular barriers, and d) transport across intracellular barriers and organelle-specific release.


Poly(phosphazene)s are a class of biodegradable materials that could provide these urgently needed characteristics to gene carriers. Pioneering work from the Allcock group established some of the key

Dr. W.-H. Hsu, Dr. E. Gomez-Ibarlucea, Prof. N. Csaba, Prof. M. Garcia-Fuentes
Center for Research in Molecular Medicine and Chronic Diseases (CIMUS) Av. Barcelona s/n
Universidade de Santiago de Compostela
15782, Santiago de Compostela, Spain
E-mail: marcos.garcia@usc.es

Dr. W.-H. Hsu, Prof. C. Alexander
Division of Molecular Therapeutics and Formulation
School of Pharmacy
University of Nottingham
Nottingham NG7 2RD, UK
E-mail: cameron.alexander@nottingham.ac.uk

Dr. P. Sánchez-Gómez
Neurooncology Unit
Instituto de Salud Carlos III (UFIEC)
Carretera de Majadahonda-Pozuelo, Km. 2.200.
28220, Majadahonda, Madrid, Spain

Dr. D. P. Ivanov, Prof. R. Rahman, Prof. A. M. Grabowska
Division of Cancer and Stem Cells
School of Medicine
Queen's Medical Centre
University of Nottingham
Nottingham NG7 2RD, UK

 The ORCID identification number(s) for the author(s) of this article can be found under <https://doi.org/10.1002/adtp.201800126>

DOI: 10.1002/adtp.201800126

pharmaceutical parameters for these materials,^[4] and recent studies have shown that poly(phosphazene)s and their variants can effectively deliver small drug molecules, proteins, and nucleic acids in a number of therapeutic settings.^[5] The versatility of poly(phosphazene) chemistry derives from the possibilities to modify a precursor, poly(dichlorophosphazene), by nucleophilic substitution. However, when preparing polymers for gene delivery, this synthetic route is problematic because most functional groups display more than two nucleophilic centers, which can result in general crosslinking of the material during derivatization reactions leading to precipitation of the partially substituted polymer. Recently, a few strategies to introduce “click” handles in poly(phosphazene)s have been reported,^[6] which might be used to circumvent this problem. In this study, we have developed a poly(phosphazene) platform, containing side-chain double-bond repeating units, and prepared a series of cationic and anionic derivatives of these via thiol–ene grafting chemistries using α , ω -aminoalkanethiols and α , ω -carboxylatoalkanethiols. By combining these materials in the presence of nucleic acids, we aimed to generate mixed polyelectrolyte complexes with sufficient positive charge to bind polynucleotides and promote cell internalization, but with the capacity to destabilize cell membranes in response to pH, and at the same time to minimize polycation-induced toxicity. These optimized complexes were expected to escape more effectively than conventional polycation/nucleic acid complexes from the endolysosomal compartment, which has been considered to be the most significant intracellular barrier to effective gene delivery.^[3b,7]

Accordingly, we have applied these gene carriers to deliver nucleic acids as a potential means to treat glioblastoma (GBM), which is a highly aggressive and malignant cancer usually classified as grade IV by the World Health Organization (WHO), in view of patients' short median survival time after diagnosis (≤ 14 months).^[8] While this prognosis has improved slightly by the introduction of the Stupp protocol treatment, that is, radiotherapy plus temozolomide (TMZ) after surgical resection of diagnosed tumors,^[9] the presence of highly resistant tumor-initiating cells (TIC) still results in limited treatment options for most patients, leading to tumor relapse and failure of the therapy. There is an urgent need for better treatment strategies, and delivery of either suicide genes or gene knockdown by siRNA are possible means by which glioblastomas could be effectively targeted. For example, previous studies have shown that inhibition of dual-specificity tyrosine phosphorylation–regulated kinase (DYRK1A) caused a loss of self-renewal capacity in several primary GBM TIC cells through preventing endocytosis-mediated degradation of epidermal growth factor receptor (EGFR) by the phosphorylation–required modulator Sprouty2.^[10] In addition, advances in surgical resection for GBM-diagnosed patients are allowing for promising strategies for in situ post-operative administration, for example, the introduction of sustained-release wafers to release anti-cancer agents in situ.^[11] In this work, we applied the poly(phosphazene) platform to deliver siRNA against DYRK1A to GBM tumors via intratumor administration and report a first proof of therapeutic efficacy in vivo in combination with an anti-neoplastic treatment.

2. Experimental Section

2.1. Materials

Hexachlorocyclotriphosphazene (99%), aluminum chloride (99.99%), triethylamine (TEA), cysteamine, 2-(dimethylamino) ethanethiol hydrochloride (DMAES), 2,2-dimethoxy-2-phenylacetophenone (DMPA), branched poly(ethyleneimine) M_w 25K (PEI), 3-mercaptopropionic acid (3MPA), 4-mercaptopbutyric acid (4MBA), 6-mercaphthohexanoic acid (6MHA), 8-mercaptooctanoic acid (8MOA), heparin sodium salt (from porcine intestinal mucosa), anhydrous tetrahydrofuran (THF), 2,2,2-trifluoroethanol (TFE), anhydrous diethylene glycol dimethyl ether (Diglyme), ethidium bromide (EtBr), poly-L-lysine (M_w 30–70 kDa) were all purchased from Sigma-Aldrich and used as received.

2.2. Synthesis of the Precursor Poly(allylamino-Phosphazene)

Poly(dichlorophosphazene) (PDCP) was prepared as previously described.^[12] A pre-dried flask was loaded with 5.0 g (14.4 mmol) of hexachlorocyclotriphosphazene and aluminum chloride as a catalyst at 5–10 wt%. The reactor was filled with high-purity nitrogen and heated to an initial temperature of 240–250 °C. After the polymerization had proceeded for 3 h, the reactor was cooled to 120 °C, and 8 mL of diglyme were injected into the reactor to solubilize the crude product and to minimize cross-linking.^[13] Aluminum chloride was removed by centrifugation (7000 g at –10 °C). The product identity was confirmed by ³¹P NMR in a co-solvent of diglyme/deuterated chloroform (1:3). Subsequent nucleophilic substitution at the chlorine phosphorus centers^[14] was performed by transferring the product supernatant into a pre-dried flask containing 50 mL of anhydrous THF, where TEA and allylamine (both 3 eq. to chlorine) were added. The reaction was carried out on ice for 24 h, and then, for additional 24 h at room temperature. For purification, the mixture of raw products was filtered to remove the trimethylamine hydrochloride and the polymer was precipitated in a co-solvent (THF/water 1:2) first and then in pure water. The precipitated polymer, allylamino-poly(phosphazene) (AAPPZ), was collected and dried in vacuo (yield \approx 4.61 g, 68%).

2.3. Synthesis of Cationic and Anionic Poly(Phosphazene)s by Thiol–Ene Reactions

After synthesis of the precursor AAPPZ, two different amine side chains were introduced to provide cationic functionality, via reaction of the thiols of cysteamine and dimethyl(aminoethanethiol) with the alkenyl side chains of the polymer. Analogous reactions to install various carboxylic acid groups were carried out using 3MPA, 4MBA, 6MHA, and 8MOA. First, AAPPZ (100 mg, 1.27 mmol of allyl groups) in 8 mL TFE was mixed with the designated mercaptoalkylamine or mercaptoalkyl carboxylic acid (3 eq. to allyl group) and flushed with nitrogen gas before adding

2,2-dimethoxy-2-phenylacetophenone (0.05 eq. to allyl groups). The thiol–ene reaction was initiated under UV irradiation ($\lambda = 365$ nm) for 3 h, and then the crude product was directly dialyzed against ultrapure water (molar mass cut-off 7 kDa) until it became a clear solution. The product was recovered as a powder by freeze-drying. The polymers were analyzed by NMR and gel permeation chromatography (GPC).

2.4. Formation of Poly(phosphazene)-Based Complexes

A bi-functional plasmid DNA (pDNA) coding for enhanced green fluorescent protein (eGFP) and luciferase from firefly *Photinus pyralis* was used throughout this work. In this pDNA, wild-type eGFP was modified to enhance the fluorescence excitation and emission at 488 nm and 507 nm, respectively. *P. pyralis* luciferase was chosen as it emits yellow-green light with maximum at 560 nm across the pH range of 7.5–8.5.

Cationic poly(phosphazene)s with different side-chain ratios of cysteamine and DMAES were dissolved in 10 mM HEPES pH 5.5. The anionic side-chain poly(phosphazene)s were dissolved in 10 mM HEPES pH 8.2. The pDNA was dissolved in ultrapure water. Complexation was performed under intense vortex mixing for 30 s at various ratios between the positively charged amines of the polymer and the negative-charged phosphates on the pDNA (N/P ratio). In the case of the mixed cationic and anionic poly(phosphazene)s, the polycationic PPZ condensed both the anionic polymers and the pDNA in one step. These polymeric complexes were characterized by their stoichiometric composition ratio, in terms of positive amines (N), negative carboxylates (C) and negative DNA phosphates (P), that is, N/C/P ratio.

2.5. Characterization

2.5.1. NMR

^1H and ^{31}P NMR spectra were recorded on Bruker 400 and DRX-500 spectrometers, respectively. ^1H diffusion-ordered spectroscopy (^1H DOSY) was recorded on Varian Inova 750 (750 MHz). Solvents used were CDCl_3 , D_2O , and MeOD. All chemical shifts were reported in parts per million (ppm) relative to tetramethylsilane (TMS) or known solvent peak positions.

2.5.2. GPC

Molar masses of polymers were determined via gel permeation chromatography using a Shimadzu Prominence UPLC system fitted with a DGU-20A5 degasser, LC-20AD, CBM-20A LITE system controller, SIL-20A autosampler, CTO-20A oven and RID-10A refractive index detector. Separations were performed on a series of Aquagel 30-40-50 (300×7.8 mm, 5 mm bead size, Agilent UK) columns fitted with a matching guard column (50×7.8 mm). The mobile phase was acidic buffer solution (1 M acetic acid and 0.3 M NaH_2PO_4) at 1 mL min^{-1} flow rate and separations were performed at 37°C . Column calibration was performed using poly(2-vinylpyridine) Easi Vials (2 mL) standards (668 Da–211 kDa, Polymer Standards Service, USA).

2.5.3. Dynamic Light Scattering and Zeta Potential Measurements

Dynamic light scattering and zeta potential measurements were performed using a Nanosizer ZS instrument (Malvern, UK) at 25°C , equipped with a He–Ne laser ($\lambda = 633$ nm) with a backscatter angle of 173° . For zeta potential, measurements were performed in 1 mM KCl. Hydrodynamic radii distributions were calculated with Malvern software. From standard auto correlation functions, diffusion coefficients were related to particle hydrodynamic radius via the Stokes equation

$$R_H = \kappa_B T / 6\pi \eta D \quad (1)$$

where R_H is the hydrodynamic radius, κ_B is the Boltzmann constant, T is the temperature, and η is the viscosity of the solvent. In addition, it was assumed that particles were spherical and non-interacting.

2.5.4. Electron Microscopy

The morphologies of the polymeric complexes were characterized by transmission electron microscopy (JEOL JEM-2010) in negative staining mode using phosphotungstic acid (PTA, 2% w/v). The complex suspensions ($10 \mu\text{L}$ of solutions at a plasmid concentration of $62.5 \mu\text{g mL}^{-1}$) were dropped onto a TEM grid (Carbon Film CF400, Electron Microscopy Sciences) and left for 5 min, when the residual sample was blotted away by capillary forces. Afterward, the PTA solution was added to the grid for 1 min, and then the grids were washed with ultrapure water and dried under low-pressure prior to TEM imaging.

2.6. Potentiometric Titration and Gel Electrophoresis

The buffering capacities of cationic and anionic poly(phosphazene)s were determined by initial dissolution of the polymer in Milli-Q water to give a concentration of 50 mM of side-chain units. The anionic polymer solutions (0.5 mL) were adjusted to pH 11 with 1 N NaOH and then titrated with 1 N HCl. In between each addition, the polymers were agitated under vortex for 30 s and allowed to stabilize for another 30 s prior to pH measurement. For cationic polymers, solutions of the same concentration were adjusted to pH 2 with 1 N HCl, and then titrated with 1 N NaOH using the same method used for the anionic polymers. pKa calculation and protonation degree (α) versus pH were calculated from the potentiometric titration curves (more information on the calculations in Supporting Information).

For estimating the binding efficiency of pDNA complexation, gel electrophoresis was performed using 1% agarose containing ($0.5 \mu\text{g mL}^{-1}$) EtBr at 110 V for 50 min. Each sample was prepared to a $30 \mu\text{L}$ volume containing 1 μg plasmid. In heparin displacement tests, each polymer/DNA complex sample was challenged with different mass ratios of heparin to plasmid, using samples at a fixed volume ($30 \mu\text{L}$) and incubated for 1 h at 37°C .

2.7. Transfection, Cytotoxicity, and Confocal Imaging on 2D Monolayer

For 2D transfection and cytotoxicity studies, U87MG cells were cultured in Dulbecco's Modified Eagle Medium (DMEM, Sigma) containing 10% fetal bovine serum, 2 mM Glutamine and 100 mg L⁻¹ penicillin-streptomycin and maintained at 37 °C under a 5% CO₂ atmosphere. For 2D culture, the cells were seeded at a density of 25 000 cells cm⁻² in 24-well plates and incubated 24 h prior to transfection. Then, polymer complexes were added at various pDNA concentrations in serum-free media (OptiMEM) and incubated for 4 h. The formulations were removed after the incubation, and cells were then cultured with fresh growth medium for an additional 48 h. Cell transfection was qualitatively assessed via fluorescence microscopy and quantified with Luciferase assay kits (from Promega). Cytotoxicity was evaluated by an MTT assay (Promega). Briefly, the transfected cells were treated with 10 µL of 12 mM MTT/PBS solution and incubated with 100 µL phenol-red free media in each well for 4 h. After the supernatant was removed, 50 µL DMSO aliquots were added to the wells, mixed and incubated for 10 min before quantification on a plate reader with absorbance wavelength set at 540 nm. For intracellular trafficking studies, U87MG cells were attached on poly-L-lysine-coated 8µ-slides (Ibidi) and treated with polymeric complexes carrying Cy5-labeled blank pDNA (prepared by Label IT kit from Mirus) at the pDNA concentration of 0.3 µg per well for 4 h. Then the medium was changed to fresh growth medium for further incubation for another 20 h. After this period, treated cells were incubated with 50 nM of LysoTracker Green (Invitrogen) and 5 µg mL⁻¹ Hoechst 33 342. Finally, confocal images (Leica SP5 X) in live cells were taken. For tracking intracellular release of pDNA, CA-PPZ was labeled with cyanine 3 (Cy3) via conjugation with Cy3-NHS (from GE) and then complexed with 6MHA-PPZ and Cy5-pDNA, forming Cy3-CA-PPZ/6MHA-PPZ: Cy5-pDNA complexes. The preparation of confocal microscopy samples was by the same method described above.

2.8. Transfection and Tomographic Scanning in a 3D Spheroid Model

For establishing 3D spheroids of U87MG cells, ultra-low attachment 96-well round-bottom plates (Corning) were seeded with 250–5000 U87MG cells per well in growth media, utilizing six replicates for each experimental condition. The plates were centrifuged at 200 rcf for 5 min to induce cell accumulation and stimulate spheroid formation. After 3 days, the spheroids were adjudged ready for transfection studies. The spheroids were treated with different polymeric complexes and with different pDNA concentrations (2 and 4 µg mL⁻¹) for 16 h in OptiMEM and then incubated in growth media for another 80 h. GFP expression in each spheroid was quantified at 96 h post treatment, via ImageJ (Fiji package) analysis directly using built-in histogram functions (Figure S9, Supporting Information). The volume of the spheroids was calculated from phase-contrast microscopic images (Nikon Eclipse Ti) using an ImageJ plugin macro that measures spheroid area (*A*) from defined regions of interest (ROI).^[15] Then, the spheroid area was used to determine the radius (*R* =

$[A/\pi]^{(1/2)}$) and calculate the volume assuming that the cell aggregates formed equivalent spheres. To quantify metabolic activity in the spheroids, a resazurin reduction assay was performed. Briefly, the spheroids were treated with resazurin (60 µM) in the growth media and incubated at 37 °C for 4 h. Following that, the 96-well plate was measured with a FlexStation II plate reader set at an excitation wavelength of 530 nm and at an emission of 590 nm. The evaluation of membrane integrity in the cell was performed using 7AAD (5 µL per well, 50 µg mL⁻¹) and fluorescence observed in the mCherry channel (Ex 560/55 and filter 630/60) of the fluorescence microscope.

The quantification of fluorescence intensity in the spheroid model was carried out via selection of ROI and comparing histogram curves of fluorescence intensity (FI) for samples and the non-treated group control (Figure S9, Supporting Information). GFP-positive counts were recorded when FIs were higher than the maximum FI of non-treated groups, set as threshold (Equation (2)). For GFP-gene transferred expression, there is no optimal positive control. For this reason, GFP expression was quantified via the percentage of GFP positive pixels. There were at least four replicates in each independent experiment and displayed data were analyzed using Prism software from four to nine independent experiments.

$$\text{GFP positive pixels \%} = \frac{\sum \text{Pixels (whose FI} > \text{threshold)}}{\sum \text{Pixels (total)}} \quad (2)$$

For 7AAD, the threshold is defined from the mean fluorescent intensity (Mean FI) in the untreated group as 0% and the mean FI of 0.5% v/v Triton X-100 treated group as 100%. The percentages of 7AAD signals of treated spheroids are expressed as below.

$$\text{Mean FI of 7AAD signals} = \frac{\sum \text{Pixel} \times \text{FI}}{\sum \text{Pixels (total)}} \quad (3)$$

7AAD positive %

$$= \frac{(\text{Mean FI of treated spheroids}) - (\text{Mean FI of non-treatment})}{(\text{Mean FI of TritonX treatment}) - (\text{Mean FI of non-treatment})} \quad (4)$$

For 3D imaging, spheroid samples were fixed with 4% paraformaldehyde first and their nuclei stained with DAPI. The fixed spheroids were loaded in appropriate glass capillaries with 1% w/v low-melt agarose. The imaging was performed by fluorescent light sheet microscopy FLSM (Light-sheet Z.1, Zeiss) and presented in the same fluorescence intensity scale using ImageJ software.

2.9. GFP/Luciferase Transfection in Xenografted Model

All in vivo experiments were approved by the Research Ethics and Animal Welfare Committee at the Instituto de Salud Carlos III, Madrid, (PROEX 224/14) in agreement with the European Union and national directives. A subcutaneous xenograft model of GBM was established as previously described.^[16] Briefly, athymic nude

Foxn1nu mice were subcutaneously injected with 1 million fresh U87MG cells in 80 μ L cultured media and 20 μ L Matrigel (BD), on both flanks. When tumor sizes reached around 100–150 mm³, polymer complexes with the GFP/Luciferase pDNA (16 μ g per tumor) were injected intratumorally. One week later, before the mice were sacrificed, they were treated with Luciferin 50 mg kg⁻¹ by IP injection. The transfected tumors were excised and imaged by an In Vivo Imaging System (IVIS).

2.10. Down-Regulation Efficiency and Clonogenic Assays

Complexes of polymers with siRNA against DYRK1A (siDYR) (ON-TARGETplus Human DYRK1A, Dharmacon) with siRNA concentration 1 μ g mL⁻¹ were added to U87MG (75K cells per well) in 12-well plates for 4 h and then maintained in culture media for 24 h. The silencing efficiency following transfection was then measured by qRT-PCR. The treated cells were collected for mRNA extraction by High-pure RNA isolation kit (from Roche) and finally, mRNAs were trapped by a glass fiber fleece in filter tubes. After elution of mRNA, the reverse transcription of 200 ng mRNA was performed by PrimeScript RT kit (from TaKaRa). The appropriate cDNA was mixed with SYBR-Green and either primers of DYRK1A (Forward 5'-3': GCAATTCCT-GCTCCTCTTG; Reverse 5'-3': TTACCCAAGGCTTGTGTCC) or primers of HPRT (Forward 5'-3': TGACACTGGCAAAACAAT-GCA; Reverse 5'-3': GGTCTTTTTCACCAGCAAGCT), used as a reference (housekeeping gene). Gene expression was measured by quantitative RT-PCR (Lightcycler-480 II, Roche).

For self-renewal assays, the silenced cells were detached and left in a serum-free medium, Neurobasal (Fisher-Scientific) supplemented with B27 (1:50), EGF (40 ng mL⁻¹) and FGF (20 ng mL⁻¹) (Peprotech) for 3 days to form spheroids. Then, the spheroids were dissociated by Accumax (Millipore) and the serum-deprived cells were seeded on 96-well plates (250 cells per well) for 7–10 days in the same serum-free medium. The numbers of secondary spheroids formed were counted.

2.11. Combination Treatment of siRNA of DYRK1A and Temozolomide in Xenograft Models

To investigate the therapeutic effectiveness of DYRK1A-silenced gene delivery in vivo, a subcutaneous xenograft model was established as described above. When tumor sizes reached around 100–150 mm³, the polymeric complexes were injected intratumorally with 4 μ g siDYR or the same amount of the scrambled sequence (siCtrl) for each tumor per day, over 4 consecutive days (total 16 μ g siRNA for each tumor, 0.6 mg kg⁻¹).^[17] On the same treatment days, mice from both study arms were also administered 5 mg kg⁻¹ TMZ by intraperitoneal injection (total dose 20 mg kg⁻¹ each mouse). The tumor sizes were measured by a caliper and calculated by Volume = $W \times W \times L/2$, in which W represents width and L is length.

2.12. Hemolysis Tests

Rat blood was collected in K2E tubes containing EDTA (BD Vacutainer) and was centrifuged at 1000 rcf for 5 min. After washing

with PBS three times under the same centrifuge conditions, the red blood cells were re-suspended either in PBS 7.4 or in PBS 5.5 at 3% (w/v) concentration. The erythrocyte suspensions were allocated across 96 wells and incubated with either CA-PPZ:pDNA or CA-PPZ/6MHA-PPZ:pDNA complexes for 2 h at 37 °C under mild shaking. Then, the plates were centrifuged and the supernatants transferred to a new plate for colorimetric analysis. The absorption of the released hemoglobin was measured in a 96-well plate reader at an excitation wavelength of 570 nm. The maximum hemolysis (positive control) was established using cells treated with 1% (v/v) Triton X-100 and the minimum value was set by treatment with PBS either at pH 7.4 or at pH 5.5.

2.13. Statistical Analysis

All data were presented as mean \pm standard error of the mean (SEM). For statistical analysis, data were transformed if required for normalization. The normality of the data was tested by a Shapiro–Wilk test. Significant differences were tested with Student's t tests or ANOVA. p -Values < 0.05 were considered to be significant, although p -values below this level are also noted in individual figures and in the text. Statistical tests applied and the number of independent replicates are noted in the figure captions. All statistical analyses were carried out via GraphPad Prism 7.

3. Results

The strategy for the synthesis of various substituted poly(phosphazene)s was via thermal ring-opening polymerization of the cyclic monomer hexachlorophosphazene (1) and reaction of the resultant PDCP with allylamine under basic conditions to afford vinylic side chains.^[6b] These were amenable to thiol–ene derivatization to yield a series of polycations and polyanions (Figure 1a).

The initially formed PDCP (2) was characterized by ³¹P NMR (Figure S1, Supporting Information), and this compound was reacted by nucleophilic substitution at the P–Cl bonds with allylamine to generate the key precursor polymer AAPPZ. A range of different cationic (4–6) and anionic (7–10) side-chain polymers (Figure 1a) were generated from AAPPZ via thiol–ene click chemistry. Reactions proceeded to a high degree ($\geq 93\%$ substitution of the allyl groups by the cationic side chains) and good overall yield ($\geq 71\%$). Product identity was confirmed by ¹H NMR (Figures S2, Supporting Information). The molar masses of the final product cysteamine-linked poly(phosphazene) (CA-PPZ, 4) were estimated by aqueous GPC, with calibration against commercial standards of poly(2-vinylpyridine). Two families of CA-PPZ polymers were characterized with molar masses of M_w 35.9 \pm 3.9 kDa (PI = 1.54) and 26.0 \pm 2.4 kDa (PI = 1.56), respectively.

The polymers were intended as nucleic acid carriers, for which their abilities to act as “proton-sponges” and/or membrane disruptors^[18] are highly dependent on their ability to accept protons and to change their hydrophilic/ lipophilic balance across intracellular pH ranges. The apparent pKa values of the polycations and polyanions were thus determined by potentiometric titrations (Figure S3, Supporting Information,

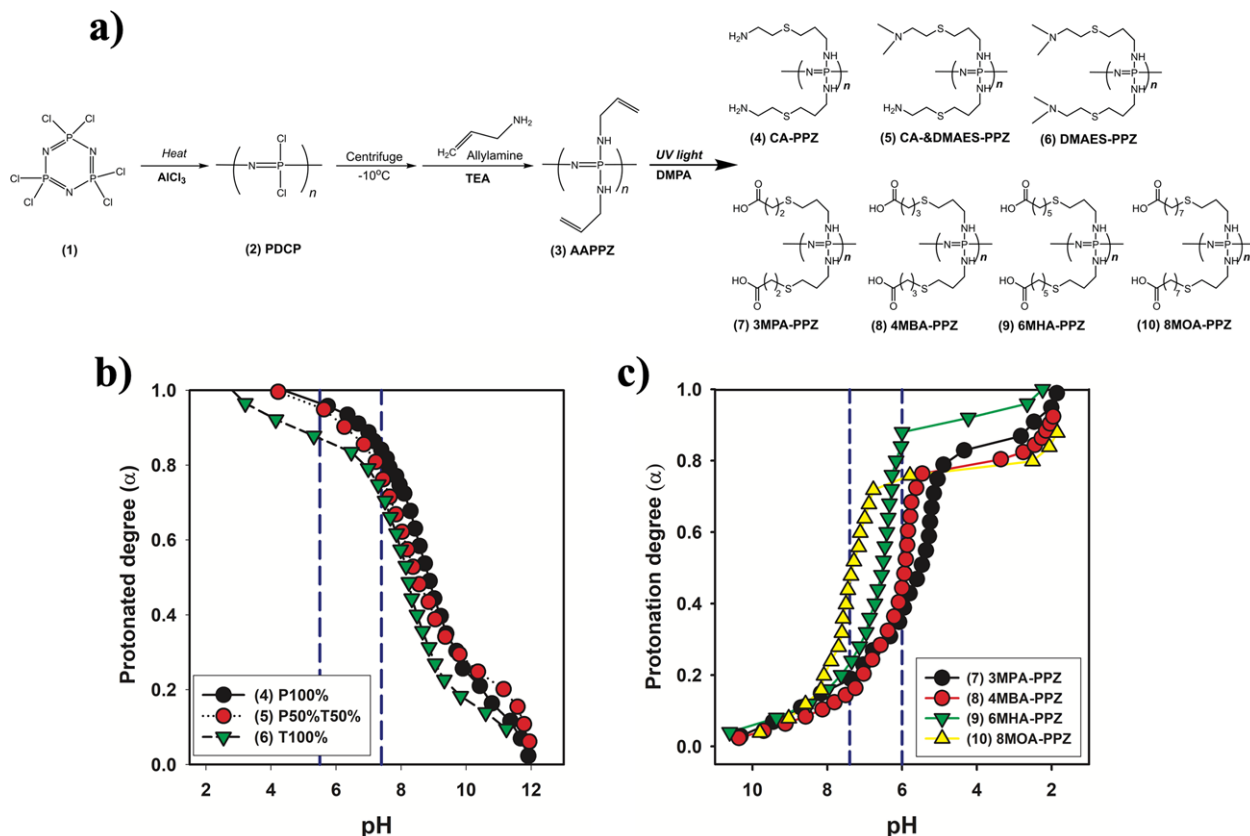


Figure 1. Synthesis and characterization of cationic and anionic poly(phosphazene)s. a) Synthesis of either cationic or anionic poly(phosphazene)s via thermal ring-opening polymerization, nucleophilic substitution and thiol-ene click chemistry. b,c) Protonation degree (α) of different cationic poly(phosphazene)s (b) and of different anionic poly(phosphazene)s (c) against pH.

and Figure 1b,c). As expected, the amine side-chain polymers remained protonated across cytosolic and endolysosomal pH ranges. However, the various aliphatic acid side-chain polymers, derived from 3-mercaptopropanoic acid (3MPA), 4-mercaptopbutanoic acid (4MBA), 6-mercaptohexanoic acid (6MHA), and 8-mercaptooctanoic acid (8MOA) exhibited buffering regions across the range of pH 5 to pH 8. These titration curves were converted to line charts plotting protonation degree (α) against pH (methods in Appendix, Supporting Information). The largest shift in protonation over the critical range of physiological pH to early endosomal pH (pH 7.4 to 6.0) was exhibited by 6MHA-PPZ with a change in α of $61.9 \pm 3.6\%$. This was significantly higher than the other anionic polymers (Table S1, Supporting Information) and suggested that this specific polymer should be the most advantageous in enhancing endosomal escape of the gene carriers.

The cationic polymers were screened for polyelectrolyte complex formation with plasmid DNA (pDNA) at varying N/P ratios (Figure S4, Supporting Information). At N/P = 8, the diameters of the complexes were all close to 80 nm and the zeta potentials close to +40 mV. When the pDNA was added to CA-PPZ in the presence of the various polyanions (at an 8:4 ratio of amines to carboxylic acids in the mixture), the diameters increased to ≈ 100 nm and the surface charges reduced to approximately +30 mV. In addition, although the size of the complexes did not increase significantly with the addition of in-

creasing amounts of the polyanion 6MHA-PPZ, the total derived count rate in the light scattering experiments increased over one order of magnitude compared to the same complexes without this anionic PPZ (Figure S4c, Supporting Information), suggesting that more compact particulate complexes were formed in the presence of polyanionic PPZs. This was supported also by TEM images showing that CA-PPZ:pDNA displayed looser structures than CA-PPZ/6MHA-PPZ:pDNA complexes (Figure 2c,d). TEM images also corroborated the measurements made by photon correlation spectroscopy and confirmed that CA-PPZ:pDNA complexes were smaller than CA-PPZ/6MHA-PPZ:pDNA complexes. Polymer/pDNA complexes were isolated from non-complexed species by high-speed centrifugation (20K rcf, 60 min) and the production yields for CA-PPZ:pDNA and CA-PPZ/6MHA-PPZ:pDNA complexes were calculated as $85 \pm 8\%$ and $97 \pm 2\%$, respectively.

Agarose gel electrophoresis experiments were performed in the absence and presence of a competing polyanion, heparin, to test the ability of the different polycationic PPZs for retaining pDNA in the form of polyelectrolyte complexes. The data indicated that progressive replacement of the primary amine CA-PPZ with tertiary amine PPZ reduced the complexation capacity with pDNA (Figure 2a) as shown by increased pDNA migration from the complexes with PPZs substituted with 50%, and particularly 100% tertiary amine groups. Complexes of CA-PPZ:pDNA and CA-PPZ/6MHA-PPZ:pDNA were also analyzed

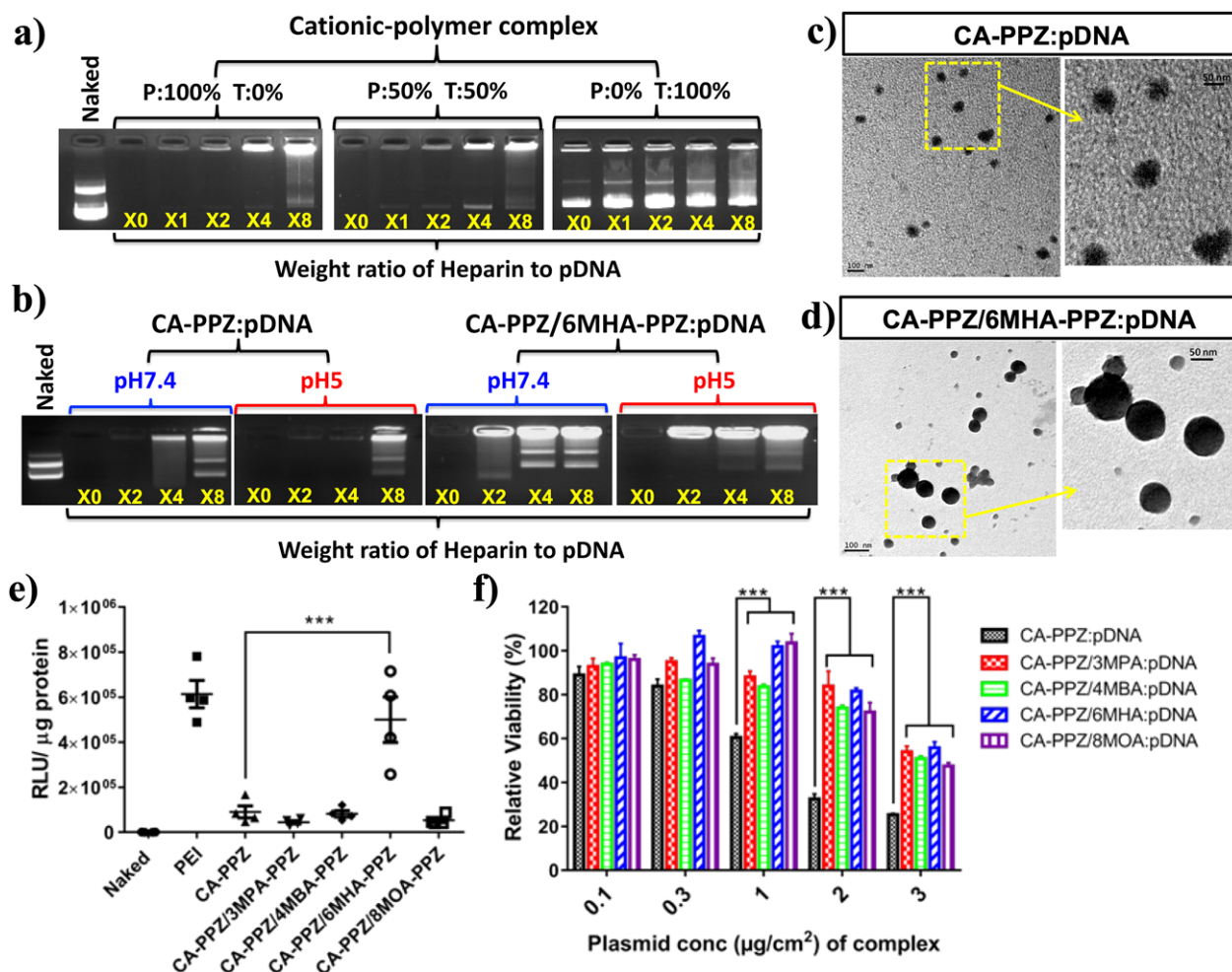


Figure 2. Design of optimized PPZ:pDNA complexes. a) Gel retardation and heparin displacement tests of complexes prepared with PPZs having 100% primary amines (P100%), P50% or P0% (8:1 N/P ratio). The remaining substitutes of each polymer correspond to tertiary amines: T0%, T50% and T100%, respectively. b) Gel electrophoresis and heparin-displacement tests of CA-PPZ:pDNA complexes and CA-PPZ/6MHA-PPZ:pDNA complexes (8:4:1 N/C/P ratio) at pH 7.4 and pH 5. c, d) TEM images of CA-PPZ:pDNA and CA-PPZ/6MHA-PPZ:pDNA complexes. e) Luciferase expression by quantification of relative luminescence unit (RLU per µg protein) obtained upon transfection of U87MG cells with CA-PPZ:pDNA complexes (8:1 N/P ratio) and different CA-PPZ/polyanionic PPZ:pDNA complexes (N/C/P ratio of 8:4:1, pDNA dose 1 µg cm⁻²) in OptiMEM (*n* ≥ 4). f) Cell metabolic activity at 48 h post treatment with different concentrations of the same complexes (*n* = 6). ****p*-value < 0.01 via one-way ANOVA analysis with Dunnett's multiple comparisons test with a single pooled variance.

by agarose gel electrophoresis and then challenged with heparin under simulated endosomal (pH 5) and standard physiological (pH 7.4) conditions (Figure 2b). There was less pDNA release from both CA-PPZ:pDNA and CA-PPZ/6MHA-PPZ:pDNA complexes at pH 5 than at pH 7, likely due to increased polymer protonation in the more acidic environment. Also, we observed that CA-PPZ associated more strongly with pDNA than the mixed CA-PPZ/6MHA-PPZ system since the latter showed more visible gel loading bands and partial pDNA migration at low heparin incubation ratios. This effect was particularly notable at pH 7.4, suggesting that 6MHA-PPZ might interact with CA-PPZ and modulate pDNA binding, especially when the 6MHA polymer became fully charged at its carboxylate functional groups.

Complexes based on cationic PPZs were initially tested for their ability to transfect U87MG glioblastoma cells when cultured as adherent monolayers. Cysteamine (primary amine)

functionalized PPZs were more effective in inducing gene expression as compared to DMAES (tertiary amine side chain) PPZs. This was likely caused by the high pDNA-binding efficiency of primary amine-poly(phosphazene) at the low N/P ratio of 8:1 (Figure 2a). In these experiments, the most favorable compromise between transfection efficiency and cell viability occurred at 8:1 N/P ratio with primary amine-PPZ:pDNA, and with the polymer of higher molecular weight (*M_w* 36 kDa) (Figure S5, Supporting Information). In order to provide for an endosomal escape mechanism, we prepared CA-PPZ:pDNA complexes which also contained polyanionic PPZs (3MPA-, 4MBA-, 6MHA-, or 8MOA-PPZ) in order to introduce aliphatic carboxylate side chains with different ionization capacity at different pH ranges. Luciferase expression assays were run in U87MG monolayers using these complexes as gene carriers, and with PEI:pDNA complexes at the same N/P ratios as a positive control (Figure 2e).

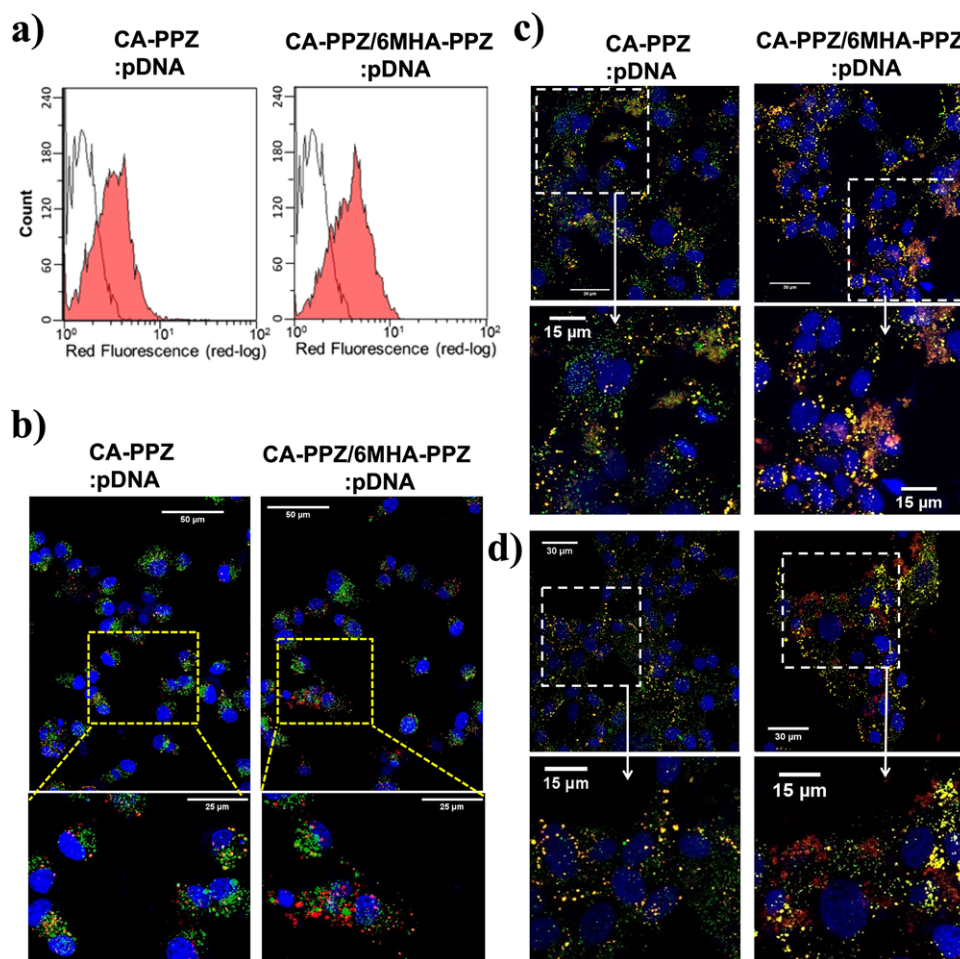


Figure 3. Comparison of the intracellular trafficking of two selected PPZ prototypes. a) Internalization of both complexes carrying Cy5-labeled pDNA after 4 h incubation with U87MG cells measured by Fluorescence Activated Cell Sorting. b) Intracellular distribution after 24 h of Cy5-labeled pDNA (red) and a late-endosome/lysosome compartment marker (Lysotracker, in green) upon delivery of CA-PPZ:pDNA or CA-PPZ/6MHA-PPZ:pDNA complexes. Intracellular distribution of Cy3-CA-PPZ (green) and Cy5-pDNA (red) after c) 24 h and d) 48 h upon delivery of CA-PPZ:pDNA or CA-PPZ/6MHA-PPZ:pDNA complexes.

The CA-PPZ/6MHA-PPZ:pDNA complexes showed the highest level of transgene expression combined with a minimal effect on cell metabolic activity as compared to the CA-PPZ:pDNA complexes. Similar enhancements in transfection were not observed in mixed complexes containing other polyanionic PPZs, indicating polymer-specific effects that we attribute to the significant change in protonation of 6MHA-PPZ at endosomal pH and in deprotonation at cytosol pH for pDNA release, especially across the early endosomal range (pH 7.4–6.0). In addition, all polyanionic PPZs reduced the cytotoxicity of the complexes, which was likely due to partial shielding of the cationic charges of CA-PPZ. The transfection enhancing effect of 6MHA-PPZ was also effective with other cationic polymers with similar structure such as poly-L-lysine (PLL), and translated to other clinically relevant glioblastoma models such as primary GBM1 cells^[19] with remarkable efficacy (Figure S6, Supporting Information). We selected 6HMA-PPZ for nanocarrier modification based on its unique ability to enhance gene transfection, a characteristic probably linked to the pKa and hydrophilic/hydrophobic balance of this

polymer. The other polyanionic polymers, 3MPA-, 4MBA- and 8MOA-PPZ, were accordingly not taken forward for the rest of this study.

To understand the performance of CA-PPZ and CA-PPZ/6MHA-PPZ complexes, internalization and intracellular trafficking were investigated by flow cytometry and confocal microscopy. CA-PPZ:pDNA and CA-PPZ/6MHA-PPZ:pDNA complexes were prepared with Cy5-labeled pDNA and incubated with U87MG cells under the same transfection conditions described previously. Flow cytometry (Figure 3a) and confocal micrographs (Figure 3b) indicated similar levels of cellular uptake for both prototypes. However, there were significant differences in the intracellular distribution of Cy5-labeled pDNA in relation to a late endosome/lysosome marker (Lysotracker, Invitrogen) between both prototypes. At 24 h post treatment, the Cy5-labeled pDNA complexed with CA-PPZ/6MHA-PPZ was more broadly distributed in the cytosol, and distal to the green-stained lysosomes. CA-PPZ:pDNA complexes remained inside lysosomes, resulting in yellow signals in the confocal merged

image (Figure 3b). The analysis of fluorescence intensities in the confocal images at 24 h post treatment indicated that the co-localization ratios (Manders' overlap coefficient as defined using the ImageJ program) of Cy5-pDNA to lysosomal markers were 0.53 ± 0.11 in CA-PPZ complexes and 0.28 ± 0.08 in CA-PPZ/6MHA-PPZ complexes, respectively, significantly different with a p -value of 0.013 via Student's t test. These data confirmed that the addition of 6MHA-PPZ facilitated the escape of the complexes from the endosomal compartment. We hypothesized that these results might be related to a capacity of 6MHA-PPZ for destabilizing biological membranes at endosomal pH. To check this hypothesis, hemolysis tests were performed at different pH values. It was found that CA-PPZ/6MHA-PPZ:pDNA complexes had no marked hemolytic effects at pH 7.4, in contrast to CA-PPZ:pDNA complexes and the internal control (PLL complexes). In contrast, CA-PPZ/6MHA-PPZ:pDNA complexes showed a clear hemolytic effect similar to those observed for PLL complexes at pH 5.5. Therefore, these experiments confirmed that CA-PPZ/6MHA-PPZ:pDNA complexes were the only systems tested which displayed pH-dependent membrane permeating properties, and the data further suggested that membrane disruption would be triggered in the endosomal compartments (Figure S7, Supporting Information). In addition to endosomal escape, intracellular distributions of the polycations and pDNA were investigated at 24 h and 48 h post treatment for both complexes to further understand pDNA release from the nanocarriers. It was observed that Cy5-labeled pDNA (red signal) was separated from Cy3-CA-PPZ/6MHA-PPZ complexes (co-localized yellow), particularly after 48 h (Figure 3c,d). On the other hand, the CA-PPZ complex retained its cargo pDNA to a much higher extent, which may be the reason why the single polycation formulations demonstrated lower transgene expression.

Following demonstration of transgene expression in 2D monolayers, we established 3D spheroids of U87MG cells as simple mimics of residual tumor regions around glioblastoma-margin areas after surgery or radiotherapy.^[20] Considering the limited penetration of excitation in microscopes and in order to exclude complicating factors of necrosis inside the spheroids, we selected small spheroids (diameter ≈ 250 μm) as our model. PPZ:pDNA complexes were assayed initially to evaluate any inherent toxicity by measuring spheroid size and metabolism through phase-contrast images and resazurin reduction assays (Alamar Blue), following the methods previously described^[15,21] (Figure S8, Supporting Information). Spheroids treated only with pDNA reduced slightly in volume after 16 h in OptiMEM media, most likely due to some nutrient depletion over this period. Incubation of the spheroids with the CA-PPZ:pDNA complexes at $4 \mu\text{g mL}^{-1}$ caused a significant decline in volume to $87 \pm 3\%$ of the initial value ($p < 0.004$) at 96 h post treatment, whereas the analogous CA-PPZ/6MHA-PPZ:pDNA complexes did not cause statistically significant reduction ($p = 0.132$) at the same dose. In resazurin reduction assays, the metabolic activities of CA-PPZ/6MHA-PPZ:pDNA-treated spheroids were slightly higher than the untreated spheroids, whereas CA-PPZ:pDNA-treated spheroids at both DNA doses ($2 \mu\text{g mL}^{-1}$ and $4 \mu\text{g mL}^{-1}$) showed no significant difference in metabolic activity compared to un-treated spheroids. These experiments indicated some possible minor toxicity for CA-PPZ:pDNA at the highest dose, and,

importantly, no signs of toxicity for CA-PPZ/6MHA-PPZ:pDNA complexes within the dose-range tested.

Further tolerability assays were performed monitoring cell membrane damage with 7-aminoactinomycin D (7AAD) on the previously used spheroid model. These experiments were performed in parallel with transgene expression level assays of GFP upon pDNA delivery with different polymer complexes (Figure 4). CA-PPZ/6MHA-PPZ successfully delivered pDNA encoding GFP as demonstrated by the percentage of GFP-positive pixels at the regions of interest (ROIs) of spheroid images ($56 \pm 8\%$ and $89 \pm 4\%$ for pDNA doses of 2 and $4 \mu\text{g mL}^{-1}$, respectively). These GFP levels were significantly higher than those obtained with CA-PPZ:pDNA and PEI:pDNA either in the fluorescent images or the quantified analysis. Regarding 7AAD staining, there were no statistically significant differences between the polymeric complexes at the same dose, and the levels were always far below those of the positive control Triton X-100. In summary, the spheroid model experiments suggested that CA-PPZ/6MHA-PPZ:pDNA complexes achieved better transfection/toxicity ratios than CA-PPZ:pDNA as well as the widely used PEI:pDNA system.

To obtain further insight into the delivery system penetration and gene transfer throughout the spheroids, fluorescence tomographic scanning was performed by fluorescent light-sheet microscopy (FLSM) (Figure 5 and tomographic-scanning videos in Supporting Information). When the spheroids were treated with complexes at the highest pDNA dose ($4 \mu\text{g mL}^{-1}$), homogeneous GFP transfection was apparent even in the core parts of the spheroids treated with CA-PPZ:pDNA and CA-PPZ/6MHA-PPZ:pDNA, although GFP fluorescence was most intense with the latter system. The lower pDNA dose ($2 \mu\text{g mL}^{-1}$) of CA-PPZ/6MHA-PPZ:pDNA complexes still provided consistent transfection throughout all the spheroid, whereas transfection with CA-PPZ and PEI:pDNA complexes was clearly less (Figure 5a). These data suggested a more efficient gene delivery for CA-PPZ/6MHA-PPZ:pDNA as compared to CA-PPZ:pDNA and the laboratory transfection standard PEI:pDNA system in this 3D model. The results also indicated that the mixed polycations/polyanion/nucleic acid system had a high capacity to penetrate through a 3D tumor structures of ≈ 250 μm in diameter. Maximum intensity projections (Figure 5b) indicated strong fluorescence throughout the spheroids transfected with the CA-PPZ/6MHA-PPZ:pDNA complexes, supporting our previous observations. Gene expression was also evaluated in larger spheroids (diameter ≥ 400 μm) where we found less transfection in the spheroid cores as compared to those tested previously (Figure S10, Supporting Information). This could be explained by two arguments. First, the nanocarriers were unable to transport to the tumor core due to the extended distance. Second, the tumor cells in the inner core of these large tumors may have been necrotic due to excessively low oxygen tension and thus be unable to produce GFP.

We next evaluated gene-transfer efficiency of the PPZ:nucleic acid complexes in centimeter-scale xenografted tumors in vivo. Nude mice were subcutaneously implanted with U87MG cells on the flanks, and when the tumors attained a size of 100–150 mm^3 , polymeric complexes with the bi-functional plasmid (encoding GFP and Luciferase) were injected intra-tumorally ($16 \mu\text{g}$ pDNA for each tumor). At the end of the experiment,

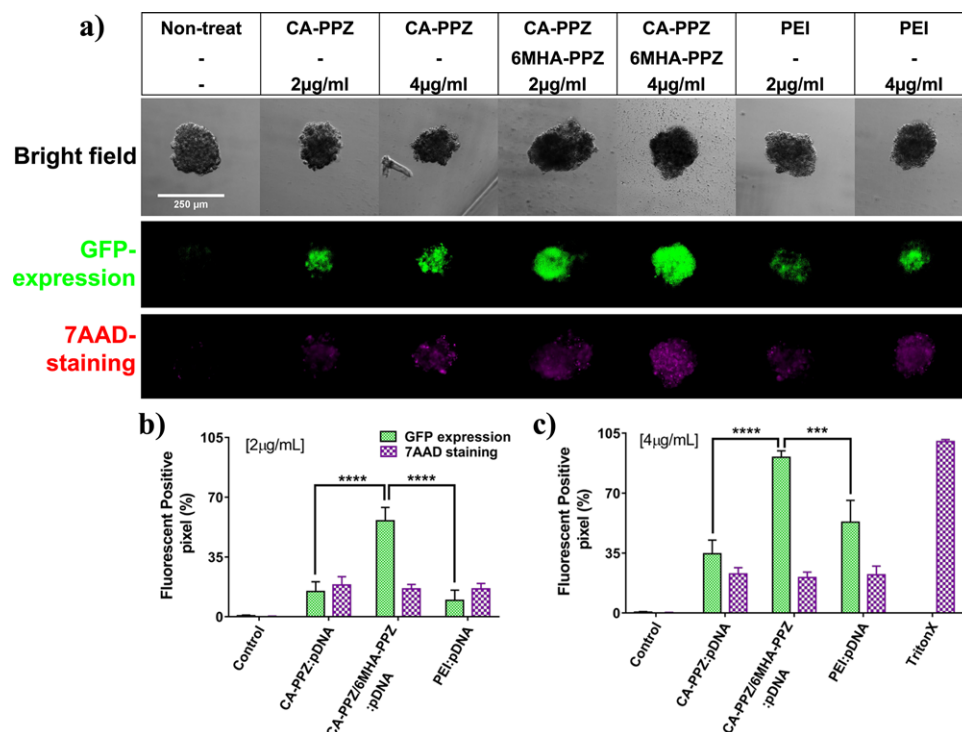


Figure 4. Transfection efficacy and viability of U87MG spheroids treated with polymeric complexes at two pDNA doses in OptiMEM. a) Overlay microscopy images showing GFP-expression and 7AAD-staining of U87MG-spheroids after treatments with CA-PPZ:pDNA (N/P 8:1) and CA-PPZ/6MHA-PPZ:pDNA (N/C/P 8:4:1) at the pDNA doses of $2 \mu\text{g mL}^{-1}$ and $4 \mu\text{g mL}^{-1}$. b,c) Quantification of GFP-fluorescence and 7AAD signals from the ROIs of spheroids in four independent experiments; spheroids treated with $2 \mu\text{g mL}^{-1}$ pDNA are analyzed in (b), those treated with $4 \mu\text{g mL}^{-1}$ pDNA in (c). (**** represents $p < 0.001$ and *** is $p < 0.01$, analyzed by a one-way ANOVA with a Dunnett's multiple comparison test with a single pooled variance; $n = 4-6$).

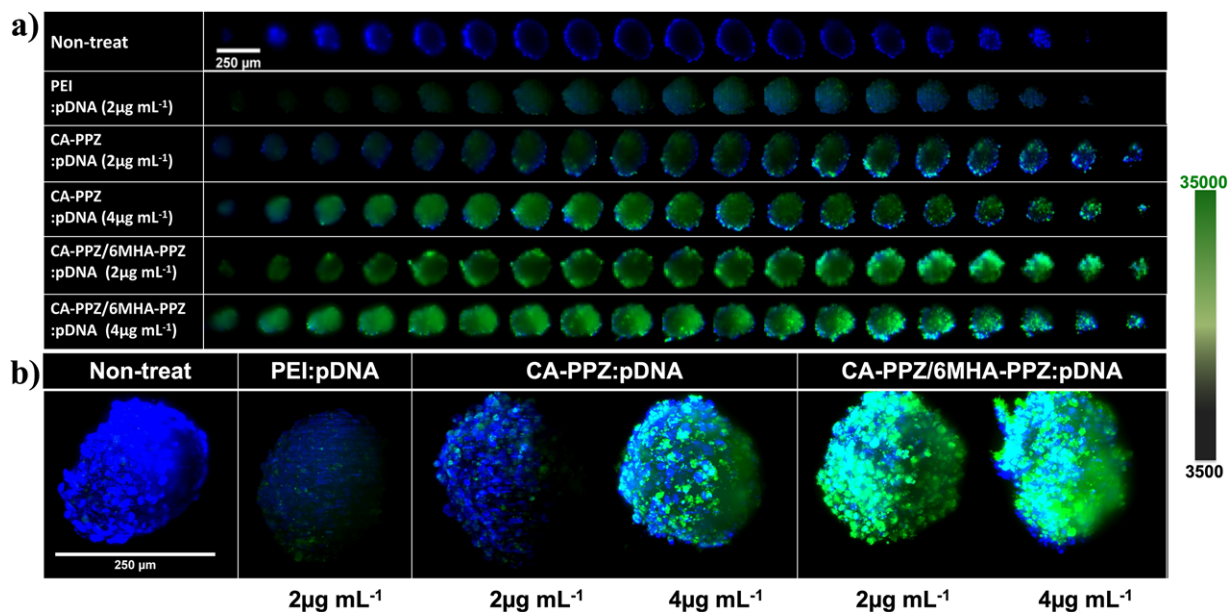


Figure 5. 3D tomographic images of GFP-transfected spheroids taken by FLSM. a) 3D section images of CA-PPZ:pDNA and CA-PPZ/6MHA-PPZ:pDNA treated spheroids (diameter $\approx 250 \mu\text{m}$) at two pDNA doses of 2 and $4 \mu\text{g mL}^{-1}$. b) Maximum intensity projections along Z-axis (XY projection) images of spheroids treated with different polymer:pDNA complexes at two doses. The images were taken by FLSM. Blue corresponds to DAPI staining; green to GFP fluorescence. The fluorescence images were analyzed by ImageJ and processed under the same scale of fluorescence intensity.

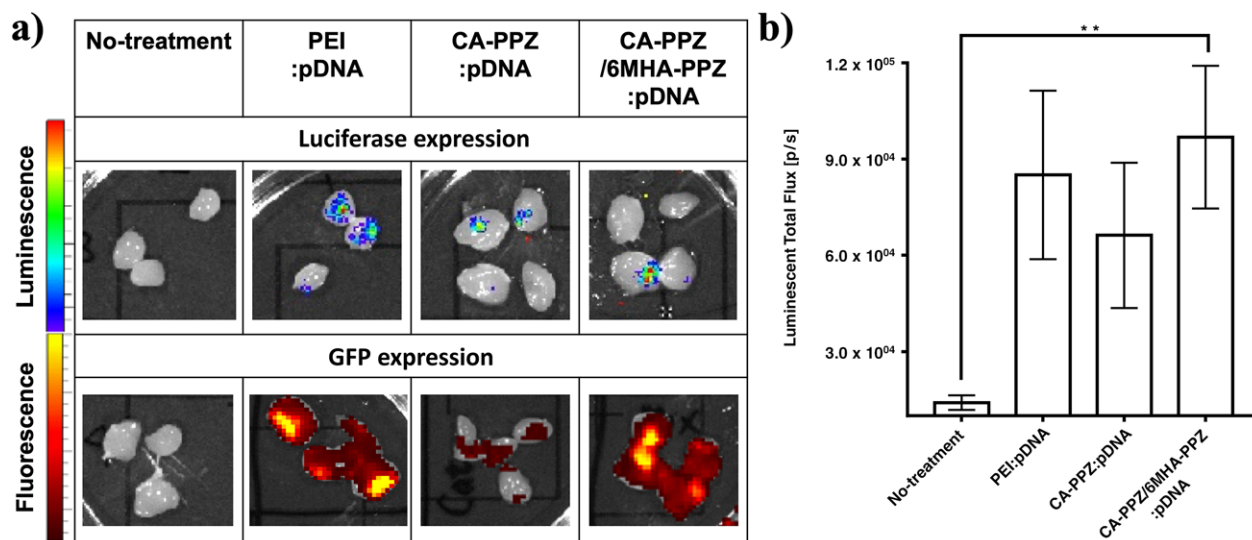


Figure 6. Transfection of polymeric complexes on xenograft tumors of U87MG. a) IVIS images of luciferase/GFP transfected U87MG tumors in nude mice. b) Quantitative analysis of the fluorescence in the ROI. **Statistically significant $p < 0.05$ via one-way ANOVA with a Dunnett's multiple comparison test ($n = 4$).

tumors were excised, sectioned, and observed by IVIS. The data indicated that the tumors were transfected by all the polymeric complexes tested, with a marked increase in luminescence compared to un-treated tumors (Figure 6a,b). ROI quantification of luciferase expression showed that CA-PPZ/6MHA-PPZ:pDNA complexes were similar in transfection efficacy to PEI-complexes and around 1.5-fold more effective than CA-PPZ:pDNA complexes (Figure 6b).

Since many of the critical properties underlying the good performance of CA-PPZ/6MHA-PPZ:pDNA nanocarriers were based on their capacity to provide transfection in 3D environments and enhance endosomal escape, we speculated that such advantages would translate to RNA delivery. Therefore, for a therapeutic transgene, we chose a small-interfering RNA to silence DYRK1A (siDYR), a gene implicated in the stability of EGFR presentation and in tumor renewal.^[10a,22] The polymer/siRNA complex formulations were made using the same composition ratio (N/C/P 8:4:1) used for the polymer/pDNA complexes above. Primary characterization showed that substitution of pDNA by siRNA did not induce substantial modifications in nanocarrier characteristics (Figure S11, Supporting Information). The DYRK1A silencing efficiency was measured by qRT-PCR of DYRK1A mRNA in U87MG 2D cell cultures (Figure 7a). CA-PPZ/6MHA-PPZ:siDYR complexes were able to silence DYRK1A expression by 70%, while the same prototype carrying a scrambled siRNA sequence (siCtrl) did not change DYRK1A expression compared to non-treated cells. In addition, CA-PPZ/6MHA-PPZ:siDYR efficacy was higher than the positive control PEI:siDYR complexes, whereas CA-PPZ:siDYR complexes did not show target inhibition. As an effect of this DYRK1A inhibition, the renewal capabilities of U87MG were diminished by the treatment with CA-PPZ/6MHA-PPZ:siDYR complexes, as observed in clonogenic assays evaluating the formation of secondary spheroids (Figure 7b). This effect on the ability to form secondary spheroids was also clear in microscopy

images (Figure 7c–e) and suggested that this gene therapy construct was capable of abrogating the tumor-initiating cell capabilities of U87MG cells.

Based on the functional experiments in vitro, the CA-PPZ/6MHA-PPZ complexes showed efficacy in reducing significantly the renewal capability of the GBM cells. We therefore selected this optimized formulation for further proof-of-concepts in vivo. Complexes of CA-PPZ/6MHA-PPZ were used to deliver siDYR (4 μ g) by intratumoral injection in combination with an intraperitoneal injection of TMZ (5 mg kg⁻¹) once per day for 4 consecutive days, in the same U87MG-xenografted mouse model (Figure 7f, red arrows). The control group was treated the same TMZ treatment and nanocarrier but with a scrambled siRNA (siCtrl) as payload. In Figure 7g, tumor growth was significantly delayed by CA-PPZ/6MHA-PPZ:siDYR complexes from day 10 to day 14 as compared to the CA-PPZ/6MHA-PPZ:siCtrl group. In fact, a statistical comparison of all the data from day 7 to 17 revealed a strong difference between the growth of tumors treated with siDYR complexes and those treated with siCtrl (i.e., growth of 4.7 ± 1.4 -fold for siDYR versus 8.7 ± 2.9 -fold for siCtrl; $p = 0.014$, Student's t test). This reduction in tumor growth rate can be better appreciated by comparing the size of the treated tumors and those of the controls on the same day (Figure 7g); tumors treated with CA-PPZ/6MHA-PPZ:siDYR were around 50% smaller than those of the control. These data underscored the potential therapeutic superiority when combining the first-line treatment TMZ with CA-PPZ/6MHA-PPZ:siDYR complexes in relation to TMZ alone.

4. Discussion

Poly(phosphazene)s have been considered as promising materials for gene delivery since they combine biodegradability with high flexibility in terms of chemical diversity. However,

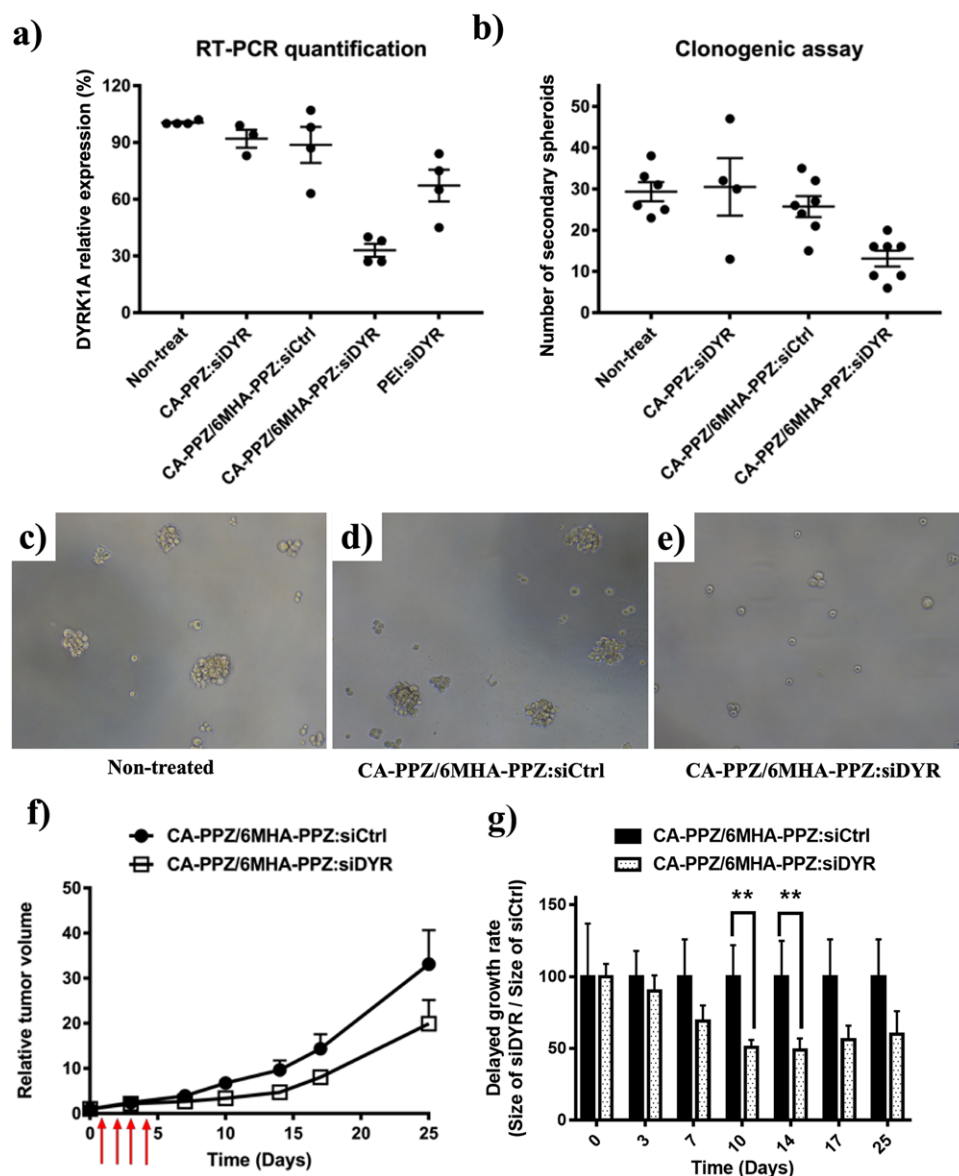


Figure 7. In vitro and in vivo silencing efficacy of polymer:siDyr complexes. a) DYRK1A silencing effect of different polymer:siRNA complexes in a 2D U87MG cell model measured by qRT-PCR. b) Clonogenic ability (formation of secondary spheroids) of U87MG cells after treatment with different polymer:siRNA complexes. Micrographs in (c, d, e) show images of secondary spheroids after treatment with CA-PPZ/6MHA-PPZ complexing either a therapeutic (siDyr) or a scrambled siRNA (siCtrl). f) Relative tumor volume in a U87MG xenograft tumor model treated with CA-PPZ/6MHA-PPZ:siCtrl or CA-PPZ/6MHA-PPZ:siDyr (4 μ g per tumor) and co-therapy with an intraperitoneal injection of TMZ 5 mg kg⁻¹. This treatment was repeated for 4 consecutive days (red arrows). g) Delayed tumor growth rate (size of siDyr treated tumors divided by the size of siCtrl treated tumors) at different time points in the same in vivo experiment ($n = 4$). ** $p < 0.05$, analyzed by unpaired Student's t test.

their application for gene delivery has remained relatively unexplored because the main synthetic route for polymer modification involves nucleophilic substitution of the precursor PDCP and is problematic for most derivatives of interest. The reason is that functional groups often present in biomedical polymers (i.e., amines, hydroxides, carboxylic acids, etc.) can crosslink the precursor PDCP. Recently, PPZs have been modified with allylamine and propargylamine as side groups that could be used as click handles in thiol-ene or thiol-yne additions.^[6b,23] Inspired by those studies, we introduced vinyl groups in our systems through

the formation of a secondary polymer precursor AAPPZ, thus enabling further modification with functional groups of interest in a simple step using a thiol-ene addition reaction. This method of generating “clickable” poly(phosphazene)s for gene delivery applications has the important advantages of requiring no protection or deprotection reactions, and enables facile and rapid preparation of multiple new derivatives with primary amines or carboxylic acid pendent groups. The streamlined synthetic process thus enabled structure/performance relationships to be derived rapidly in terms of in vitro transgene expression efficiency.

An important finding from the initial screening experiments was the identification of 6MHA-PPZ as a material with gene delivery enhancing properties. This polymer was designed to perform three different functions in the delivery system: i) improve interpolymer complexation during the formation of the mixed polyelectrolyte, ii) promote the release of polynucleotides from endolysosomal compartments, and iii) reduce polycation-caused toxicity. The capacity of anionic PPZs to enhance interpolymer complexation was confirmed by comparing CA-PPZ:pDNA (8:1 N/P ratio) and CA-PPZ/6MHA-PPZ:pDNA (8:4:1 N/C/P ratio) complexes via dynamic light scattering and TEM imaging. Dynamic light scattering showed almost a one order of magnitude increase in derived count rate when 6MHA-PPZ was added (Figure S4c, Supporting Information). TEM images showed that CA-PPZ/6MHA-PPZ:pDNA complexes had more compact morphologies than CA-PPZ:pDNA complexes (Figure 2c,d). Many standard polymers used for gene delivery are typically used in excess to the polynucleotide. For example, while it is necessary only to use an N/P ratio of 3 when aiming to form colloiddally stable complexes of pDNA with PEI, in practice, larger amounts of PEI are used for improving in vitro transfection efficiency, thus resulting in weakly bound or unbound PEI.^[24] However, there are concerns regarding the fate and side effects of these unbound polymers when these systems are administered in vivo. In comparison, the dense network of the CA-PPZ/6MHA-PPZ:pDNA complexes as shown in the TEM images suggested that these formulations were more closely associated and thus more likely to be delivered as intact complexes to the target cells.

A second observation regarding the function of 6MHA-PPZ in the nanocomplexes was its capacity to increase the efficacy/toxicity ratio over one order of magnitude, reaching levels similar to the laboratory transfection standard PEI:pDNA in 2D models of U87MG cells (Figure 2e), and showing superior efficacies in a clinically relevant glioblastoma primary cell-line (GBM1, Figure S6, Supporting Information). Indeed, we observed that introduction of all polyanionic-PPZs in the complexes reduced the overall cellular toxicity. We infer that this reduction was partly driven by charge neutralization, an effect already reported with other polyanions.^[25] However, the other polyanionic PPZs failed to enhance the efficacy of gene delivery compared to 6MHA-PPZ (Figure 2e). Microscopy showed that the presence of 6MHA-PPZ in the complexes resulted in lower co-localization with the endosomal compartments (Figure 3b), suggesting that this improvement in transfection could be related to higher capacity of these formulations to exit the endosomal vesicles. Since this improvement in transfection was specific for 6MHA-PPZ, we think it resulted from the change in ionization degree of 6MHA-PPZ across the early endosomal pH range, which was the largest among all the polyanions we tested (Table S1, Supporting Information, and Figure 1c). This change in ionization was most probably linked to the capacity of 6MHA-PPZ to rupture lipid membranes in the acid environment of the endosomes as confirmed in hemolysis tests (Figure S7, Supporting Information). Complexes containing 6MHA-PPZ were the only ones that exhibited negligible hemolytic effects at neutral pH, but a hemolytic effect comparable to PLL at acidic pH. It is also of note that 6MHA-PPZ was capable of improving cell transfection when combined with polycations known to possess low endosomal escape properties, such as PLL, although the combination with CA-PPZ was the most ef-

ficient in the different cell-lines (Figure S6, Supporting Information), likely related to the specific optimization performed (Figure S5a,b, Supporting Information).

Traditional 2D cell monolayer models have been widely used for optimization of formulations, but also have been questioned for their ability to represent physiologically relevant situations. Three-dimensional cultures are better able to provide tissue-like architectures (e.g., extracellular matrix, cell interactions),^[26] fundamental tumor microenvironment traits such as nutrient and oxygen gradients,^[27] and also gene expression profiles similar to those of clinical tumors.^[28] To date, very few studies have investigated nucleic acid delivery in tumor spheroids despite the fact that they are highly suited as preliminary assays before in vivo efficacy studies and that they can provide critical information regarding tumor penetration, which is a critical barrier in cancer drug delivery.^[29] For our investigations, we used FLSM to obtain tomographic fluorescence images of GFP transfection expression without damaging the initial spheroid structure. As apparent in Figure 5, CA-PPZ/6MHA-PPZ:pDNA complexes exhibited higher transfection in GBM spheroids as compared to CA-PPZ:pDNA and the reference PEI:pDNA complexes; this difference was particularly marked at low pDNA doses. This improved efficacy was also accompanied by reduced toxicity. Overall, these results showed high transfection efficacy and tumor penetration capacity for the CA-PPZ/6MHA-PPZ:pDNA formulation, which we attribute to their partially neutralized cationic charges at physiological pH and lower tendency to bind to the extracellular matrix in tumor spheroids. The results were also in agreement with those from subsequent in vivo gene delivery experiments, although direct correlation between these assays is problematic due to inhomogeneous transfection levels observed distal of the injection sites (Figure 6).

GBM-initiating cells are considered to be responsible for tumor recurrence,^[30] and therefore, their suppression is essential for any medicine intended to provide mid- or long-term survival benefits. In the past, we have shown that controlled release implants can deliver glioblastoma-initiating cell suppressing molecules and provide a therapeutic benefit in advanced in vivo models.^[31] Because the critical properties behind the performance of this formulation are barriers common to both pDNA and siRNA delivery (i.e., endosomal escape, transfection in 3D environments), following the pilot in vivo study with pDNA, we applied the optimized polymer prototype to deliver a siRNA sequence with known activity against glioblastoma-initiating cells (siDYR).^[10a] As in the case of the DNA complexes, the use of 6MHA-PPZ mixed in with the CA-PPZ complexes provided sufficient ionic attraction for complexation, and as a result the physicochemical properties of CA-PPZ/6MHA-PPZ:siRNA were similar to CA-PPZ/6MHA-PPZ:pDNA (Figure S11, Supporting Information). We also confirmed that protein silencing observed for cells treated with CA-PPZ/6MHA-PPZ:siDYR resulted in a reduction in the clonogenic index in a secondary spheroid formation assay, indicating the abrogation of the "initiating cell" phenotype of the target cells, an effect that could have major clinical relevance in combination therapies. Since we expect gene therapy to provide initial clinical benefits in neuro-oncology as adjuvants in combination with antitumoral drugs, the CA-PPZ/6MHA-PPZ:siDYR formulation was evaluated in U87MG xenografted mice, in a therapeutic scheme including co-delivery of the

first-line treatment TMZ. The experiment showed a significant delay in tumor progression in the treatment arm receiving TMZ and CA-PPZ/6MHA-PPZ:siDYR versus the control arm receiving TMZ and CA-PPZ/6MHA-PPZ complexed with a scrambled siRNA sequence (Figure 7f,g). Therefore, our results indicate an additional therapeutic benefit for the combination of CA-PPZ/6MHA-PPZ:siDYR gene therapy with the standard pharmacological GBM treatment, as compared to this standard treatment alone. Further studies will be needed to elucidate the possible clinical impact of this combined therapy in more advanced models and performing additional phenotypic analysis in the tumors.

5. Conclusion

A synthetic strategy for the simple preparation of a small library of poly(phosphazene)s of interest for gene delivery was developed based on the precursor polymer with “clickable” sites, and further derivation by thiol–ene additions. This approach allowed us to test a variety of compounds and draw structure/function relationships for gene delivery. Based on the screenings, a primary amine-containing polymer (CA-PPZ) and an anionic poly(phosphazene) analogue (6MHA-PPZ) were selected for plasmid DNA gene delivery. These binary polymer/pDNA complexes displayed significantly higher transfection efficiencies than the parent polycation-only system in 2D monolayers, 3D spheroids of U87MG cells and in a subcutaneous xenograft model, due to improved tumor transport and intracellular trafficking characteristics. This optimized prototype also showed indications of superior performance compared to laboratory standard PEI complexes, particularly in 3D tumor models. When used for RNAi therapy, CA-PPZ/6MHA-PPZ complexes efficiently delivered siRNA against DYRK1A in U87MG cells, inducing a significant reduction of their self-renewal capability in vitro and a significant anti-tumor effect in an in vivo glioblastoma model. Overall, the data established a new versatile, biodegradable polymeric gene delivery based on poly(phosphazene)s with high capacity for gene-transfer efficacy in vitro and upon in-situ treatment in vivo.

Supporting Information

Supporting Information is available from the Wiley Online Library or from the author.

Acknowledgements

The authors thank the European Commission for an Erasmus Mundus grant to WHH (NanoFar Joint Doctorate Program). This work was funded by the Engineering and Physical Sciences Research Council [Grants EP/H005625/1, EP/N03371X/1] and the Royal Society (Wolfson Research Merit Award WM150086) to C.A., Ministerio de Economía y Competitividad (MINECO-RETOS, Grant SAF2015-65175-R to P.S.G. and SAF2014-58189-R to M.G.-F, FEDER Funds) and Fundación BBVA 2014-PO0110 to M.G.F. The pEGFP-Luc plasmid DNA was a kind gift from Prof. A. Vidal and Dr. C. Carneiro (University of Santiago de Compostela). The primary GBM cell-line GBM1 was a kind donation from Dr. M. D. Bernard Rogister (University of Liege). The authors acknowledge Pamela Collier, Christine Grainger-Boulton, Paul Cooling, Dr. Manuel Martin-Pastor, and Dr. Jose

Manuel Ageitos for expert technical support. The authors also appreciate help from Dr. Esther Hernández and Paloma Fernández in molecular biological assays and in vivo studies.

Conflict of Interest

The authors declare no conflicts of interest.

Keywords

click chemistry, glioblastoma, polymeric gene delivery, poly(phosphazene)s, siRNA delivery, tumor-initiating cells

Received: September 26, 2018

Revised: November 13, 2018

Published online:

- [1] a) A. N. Zelikin, C. Ehrhardt, A. M. Healy, *Nat. Chem.* **2016**, *8*, 997; b) R. Kanasty, J. R. Dorkin, A. Vegas, D. Anderson, *Nat. Mater.* **2013**, *12*, 967; c) H. Yin, R. L. Kanasty, A. A. Eltoukhy, A. J. Vegas, J. R. Dorkin, D. G. Anderson, *Nat. Rev. Genet.* **2014**, *15*, 541.
- [2] R. Titze-de-Almeida, C. David, S. S. Titze-de-Almeida, *Pharm. Res.* **2017**, *34*, 1339.
- [3] a) C. Scholz, E. Wagner, *J. Controlled Release* **2012**; b) A. Krivitsky, D. Polyak, A. Scamparin, S. Eliyahu, A. Ori, S. Avkin-Nachum, V. Krivitsky, R. Satchi-Fainaro, *Biomacromolecules* **2016**, *17*, 2787; c) S. M. Moghimi, E. Wagner, *Mol. Ther.* **2017**, *25*, 1461; d) U. Lachelt, E. Wagner, *Chem. Rev.* **2015**, *115*, 11043.
- [4] H. R. Allcock, *Science* **1976**, *193*, 1214.
- [5] a) A. P. Martinez, B. Qamar, T. R. Fuerst, S. Muro, A. K. Andrianov, *Biomacromolecules* **2017**, *18*, 2000; b) Y. Peng, X. M. Zhu, L. Y. Qiu, *Biomaterials* **2016**, *106*, 1; c) M. H. Gao, X. M. Zhu, L. P. Wu, L. Y. Qiu, *Biomacromolecules* **2016**, *17*, 2199; d) C. Y. Ma, X. Zhang, C. G. Du, B. J. Zhao, C. H. He, C. Li, R. Z. Qiao, *Bioconjugate Chem.* **2016**, *27*, 1005; e) L. J. Meng, C. Q. Xu, T. H. Liu, H. Li, Q. H. Lu, J. G. Long, *Polym. Chem.* **2015**, *6*, 3155; f) I. Teasdale, O. Bruggemann, *Polymers* **2013**, *5*, 161; g) P. C. Zhang, Z. W. Zhang, Y. X. Yang, Y. P. Li, *Int. J. Pharm.* **2010**, *392*, 241.
- [6] a) X. Huang, X. J. Huang, A. G. Yu, C. Wang, Z. W. Dai, Z. K. Xu, *Macromol. Chem. Phys.* **2011**, *212*, 272; b) Y. C. Qian, X. J. Huang, C. Chen, N. Ren, X. Huang, Z. K. Xu, *J. Polym. Sci., Part A: Polym. Chem.* **2012**, *50*, 5170.
- [7] a) A. K. Varkouhi, M. Scholte, G. Storm, H. J. Haisma, *J. Controlled Release* **2011**, *151*, 220; b) T. Endoh, T. Ohtsuki, *Adv. Drug Delivery Rev.* **2009**, *61*, 704; c) H. C. Kang, Y. H. Bae, *Adv. Funct. Mater.* **2007**, *17*, 1263.
- [8] E. G. Van Meir, C. G. Hadjipanayis, A. D. Norden, H. K. Shu, P. Y. Wen, J. J. Olson, *Ca-Cancer J. Clin.* **2010**, *60*, 166.
- [9] a) M. Westphal, D. C. Hilt, E. Bortey, P. Delavault, R. Olivares, P. C. Warnke, I. R. Whittle, J. Jääskeläinen, Z. Ram, *Neuro-Oncology* **2003**, *5*, 79; b) R. Stupp, W. P. Mason, M. J. Van Den Bent, M. Weller, B. Fisher, M. J. Taphoorn, K. Belanger, A. A. Brandes, C. Marosi, U. Bogdahn, *N. Engl. J. Med.* **2005**, *352*, 987.
- [10] a) N. Pozo, C. Zahonero, P. Fernández, J. M. Liñares, A. Ayuso, M. Hagiwara, A. Pérez, J. R. Ricoy, A. Hernández-Laín, J. M. Sepúlveda, *J. Clin. Invest.* **2013**, *123*, 2475; b) S. R. Ferron, N. Pozo, A. Laguna, S. Aranda, E. Porlan, M. Moreno, C. Fillat, S. de la Luna, P. Sánchez, M. L. Arbonés, *Cell Stem Cell* **2010**, *7*, 367.
- [11] a) F. J. Attenello, D. Mukherjee, G. Datoo, M. J. McGirt, E. Bohan, J. D. Weingart, A. Olivi, A. Quinones-Hinojosa, H. Brem, *Ann. Surg.*

- Oncol.* **2008**, 15, 2887; b) M. J. McGirt, K. D. Than, J. D. Weingart, K. L. Chaichana, F. J. Attenello, A. Olivi, J. Laterra, L. R. Kleinberg, S. A. Grossman, H. Brem, *J. Neurosurg.* **2009**, 110, 583.
- [12] Y. S. Sohn, Y. H. Cho, H. Baek, O.-S. Jung, *Macromolecules* **1995**, 28, 7566.
- [13] A. K. Andrianov, J. Chen, M. P. LeGolván, *Macromolecules* **2004**, 37, 414.
- [14] Y.-C. Qian, P.-C. Chen, G.-J. He, X.-J. Huang, Z.-K. Xu, *Molecules* **2014**, 19, 9850.
- [15] D. P. Ivanov, T. L. Parker, D. A. Walker, C. Alexander, M. B. Ashford, P. R. Gellert, M. C. Garnett, *PLoS One* **2014**, 9, e103817.
- [16] C. Zahonero, P. Aguilera, C. Ramírez-Castillejo, M. Pajares, M. V. Bolós, D. Cantero, A. Perez-Nuñez, A. Hernández-Lain, P. Sánchez-Gómez, J. M. Sepúlveda, *Mol. Cancer Ther.* **2015**, 14, 1548.
- [17] K. T. Love, K. P. Mahon, C. G. Levins, K. A. Whitehead, W. Querves, J. R. Dorkin, J. Qin, W. Cantley, L. L. Qin, T. Racie, *Proc. Natl. Acad. Sci. USA* **2010**, 107, 1864.
- [18] T. F. Martens, K. Remaut, J. Demeester, S. C. De Smedt, K. Braeckmans, *Nano Today* **2014**, 9, 344.
- [19] J. Kroonen, J. Nassen, Y. G. Boulanger, F. Provenzano, V. Capraro, V. Bours, D. Martin, M. Deprez, P. Robe, B. Rogister, *Int. J. Cancer* **2011**, 129, 574.
- [20] P. J. Kelly, *Surg. Neurol. Int.* **2010**, 1, 96.
- [21] D. P. Ivanov, A. M. Grabowska, *Sci. Rep.* **2017**, 7, 41160.
- [22] a) R. Abbassi, T. G. Johns, M. Kassiou, L. Munoz, *Pharmacol. Ther.* **2015**, 151, 87; b) P. Fernandez-Martinez, C. Zahonero, P. Sanchez-Gomez, *Mol. Cell. Oncol.* **2015**, 2, e970048.
- [23] N. Ren, X. J. Huang, X. Huang, Y. C. Qian, C. Wang, Z. K. Xu, *J. Polym. Sci., Part A: Polym. Chem.* **2012**, 50, 3149.
- [24] a) S. Boeckle, K. von Gersdorff, S. van der Piepen, C. Culmsee, E. Wagner, M. Ogris, *J. Gene Med.* **2004**, 6, 1102; b) Y. Yue, F. Jin, R. Deng, J. Cai, Y. Chen, M. C. Lin, H.-F. Kung, C. Wu, *J. Controlled Release* **2011**, 155, 67.
- [25] a) L. Han, C. Tang, C. Yin, *Biomaterials* **2013**, 34, 5317; b) T. Kurosaki, T. Kitahara, S. Fumoto, K. Nishida, J. Nakamura, T. Niidome, Y. Kodama, H. Nakagawa, H. To, H. Sasaki, *Biomaterials* **2009**, 30, 2846; c) V. Trubetskoy, S. Wong, V. Subbotin, V. Budker, A. Loomis, J. Hagstrom, J. Wolff, *Gene Ther.* **2003**, 10, 261.
- [26] S. A. Enam, E. Klaus, *Neurosurgery* **1998**, 42, 599.
- [27] R. M. Sutherland, B. Sordat, J. Bamat, H. Gabbert, B. Bourrat, W. Mueller-Klieser, *Cancer Res.* **1986**, 46, 5320.
- [28] P. D. W. Hamer, A. Van Tilborg, P. Eijk, P. Sminia, D. Troost, C. Van Noorden, B. Ylstra, S. Leenstra, *Oncogene* **2008**, 27, 2091.
- [29] a) J. Zhou, T. R. Patel, R. W. Sirianni, G. Strohbehn, M.-Q. Zheng, N. Duong, T. Schafbauer, A. J. Huttner, Y. Huang, R. E. Carson, *Proc. Natl. Acad. Sci. USA* **2013**, 110, 11751; b) E. Song, A. Gaudin, A. R. King, Y.-E. Seo, H.-W. Suh, Y. Deng, J. Cui, G. T. Tietjen, A. Huttner, W. M. Saltzman, *Nat. Commun.* **2017**, 8, 15322.
- [30] C. Garcia-Mazas, N. Csaba, M. Garcia-Fuentes, *Int. J. Pharm.* **2017**, 523, 490.
- [31] a) E. Reguera-Nuñez, C. Roca, E. Hardy, M. de la Fuente, N. Csaba, M. Garcia-Fuentes, *Biomaterials* **2014**, 35, 2859; b) P. González-Gómez, J. Crecente-Campo, C. Zahonero, M. de la Fuente, A. Hernández-Lain, H. Mira, P. Sánchez-Gómez, M. Garcia-Fuentes, *Oncotarget* **2015**, 6, 10950.